Manuscript Details

Manuscript number	EABE_2018_14
Title	Debonding of FRP and thin films from an elastic half-plane using a coupled FE-BIE model
Article type	Full Length Article

Abstract

A Finite Element-Boundary Integral Equation (FE-BIE) coupling method is proposed to investigate a flexible bar weakly attached to an elastic orthotropic half-plane. Firstly, the analysis has been conducted assuming interfacial displacements linearly proportional to tangential traction for a bar subjected to horizontal force or thermal load. Secondly, the study has been addressed to model debonding behaviour of a composite reinforcement glued on a substrate. Using incremental nonlinear analysis, a bilinear elastic-softening relationship between interfacial traction and slip has been implemented in the model simulating the delamination of pure Mode II. Finally, influence of the anchorage length on the ultimate bearing capacity of the adhesive joint has been investigated.

Keywords	Mixed variational principle; Green function; Weak interface; Debonding; FRP–strengthening concrete
Taxonomy	Integral Equation, Two-dimensional Theory, Debonding, Finite Element Methods
Corresponding Author	Nerio Tullini
Order of Authors	Enrico Tezzon, Antonio Tralli, Nerio Tullini
Suggested reviewers	Enzo Martinelli, Marco Paggi

Submission Files Included in this PDF

File Name [File Type]

TezzonTralliTullini_Text.doc [Manuscript File]

TezzonTralliTullini_Figs.doc [Figure]

To view all the submission files, including those not included in the PDF, click on the manuscript title on your EVISE Homepage, then click 'Download zip file'.

Debonding of FRP and thin films from an elastic half-plane using a coupled FE-BIE model

Enrico Tezzon, Antonio Tralli, Nerio Tullini*

Department of Engineering, University of Ferrara, Via Saragat 1, Ferrara, Italy

e-mail: enrico.tezzon@unife.it; antoniomichele.tralli@unife.it; nerio.tullini@unife.it

*corresponding author

ABSTRACT

A Finite Element-Boundary Integral Equation (FE-BIE) coupling method is proposed to investigate a flexible bar weakly attached to an elastic orthotropic half-plane. Firstly, the analysis has been conducted assuming interfacial displacements linearly proportional to tangential traction for a bar subjected to horizontal force or thermal load. Secondly, the study has been addressed to model debonding behaviour of a composite reinforcement glued on a substrate. Using incremental nonlinear analysis, a bilinear elastic-softening relationship between interfacial traction and slip has been implemented in the model simulating the delamination of pure Mode II. Finally, influence of the anchorage length on the ultimate bearing capacity of the adhesive joint has been investigated.

Keywords: Mixed variational principle, Green function, Weak interface, Debonding, FRP–strengthening concrete.

1 INTRODUCTION

In the last few decades, repairing and strengthening of existing structures made of concrete and masonry [1] or rehabilitation of steel structures [2] have emerged as a cutting edge issue in structural engineering. Particularly, the use of Fibre Reinforced Polymer (FRP) strips has become more and more common than ever before, as it has proved to be a rapid and efficient technical solution. Plenty of these studies have been focused on the issue of strengthening Reinforced Concrete (RC) members with externally bonded FRP sheets [3]. Nonetheless, thin film-based devices and coated systems have been widely employed, remarkably in fields of aerospace and electronic engineering. For these problems, a simple reference model may be a straight elastic stiffener of prescribed length bonded to an elastic substrate in plane state that can debond in pure mode II only. Moreover, bending stiffness of the stiffener may be disregarded because of its thickness that is generally very small. Consequently, the stiffener is not able to sustain transverse loads and no peeling stresses can arise at the interface.

In 1932, Melan studied the problem of a point force applied to an infinite stiffener bonded to an infinite linear elastic sheet [4]. Several authors have reconsidered and extended the Melan's problem, especially for stiffened plate in aircraft structures and FRP strengthened RC structures. Early studies, concerning stiffeners welded to an elastic substrate, have adopted series approximation method to solve singular integral equations including proper Green function, see [5] and references cited therein. Perfect adherence hypothesis was relaxed in [6], where the adhesive interface was substituted by a set of independent linear elastic springs. This classical assumption [7] is frequently referred to as weak or imperfect interface and for a soft thin adhesive connecting two adherents was justified making use of asymptotic expansion methods of the corresponding three-dimensional elastic problem [8]. Nevertheless, correction terms may be required at the adhesive ends [9]. With reference to the FRP plates glued on rigid substrate, a closed-form analytical solution of shear-out test has been presented in [10], where an elastic-softening bilinear bond law describes the adhesive interface and fracture behaviour in Mode II is assumed throughout the interface. In the

same framework, the effect of the substrate elasticity has been considered in [11, 12], using a series approximation method. Alternatively, stress analysis combined with linear elastic fracture mechanics can be chosen to evaluate critical delamination condition for RC beams strengthened with FRP strips [13].

Fracture behaviour involving the substrate has required Finite Element (FE) procedures based on continuum damage models, where failure in a zone below the adhesive/concrete interface might occurred [14, 15, 16]. Accurate results have been obtained in [17, 18] using a regularized extended FE approach to study delamination test in FRP strengthened concrete. Nonetheless, the FE approach undergoes important limitations when applied to film-substrate systems [19] because a refined mesh has to be used to describe thin layer of the film. Furthermore, in order to simulate the half-plane, FE meshes should be extended to a region significantly greater than the contact area, with detrimental effect on the time needed to carry out the numerical simulations.

Boundary Element (BE) techniques can be used to evaluate the mechanical behaviour of coated systems involving thin layers, as long as the nearly-singular integrals arising in the BE formulations are handled correctly [20]. Symmetric Galerkin boundary element techniques for solving cohesive interface problems are presented in [21, 22], where the non-linear behaviour has been localized at the interface only. Moreover, in [22] both the substrate and the reinforcement has been considered as linear elastic bodies and a bar model has shown computationally more efficient than that of a thin layer.

For bars and beams resting on two-dimensional substrate, a Finite Element-Boundary Integral Equation (FE-BIE) coupling method can be suited well to give very accurate solutions at low computational cost. To date, several problems have been analysed: thin film bonded to an isotropic elastic substrate and subjected to thermal variation or axial loads [23]; Euler-Bernoulli and Timoshenko beams in frictionless [24, 25] or adhesive contact [26, 27] with an elastic half-plane, including buckling problems [28, 29]. In particular, the FE-BIE coupling method makes use of a mixed variational formulation including the Green function of the substrate and assumes as

independent fields both the nodal displacements and the contact tractions. It is worth noting that only the structure in contact with the substrate boundary has to be discretized. In addition, the mechanical response of the half-plane is represented through a weakly singular integral equation, which solution is given analytically, avoiding singular and hyper-singular integrals typically involved in the classical BE formulation. For the mixed problem at hand, useful mathematical references are in [30, 31], where well-posedness of the variational problem and of the corresponding Galerkin solution is set in a proper abstract functional framework.

In this paper, the FE-BIE coupling method is used introducing a slip between a flexible bar and an elastic orthotropic half-plane. First, the slip is assumed linearly proportional to the interface reactions. Point force and uniform thermal variation applied at a bar are investigated. To the authors' knowledge, the present proposal represents a new contribution.

In the second part of this paper, incremental nonlinear analysis of the proposed model is adopted to investigate the delamination of a FRP strengthened RC substrate. The analysis of the interfacial reaction turns out to be an important aspect about the prediction of detachment phenomenon. Extremely arduous is the representation of mechanical properties of an adhesive, which can be obtained by shear-out tests adopting different layouts, such as single slipping test with fixed back side or double pull-out shear schemes [32, 33]. Simple formulations are generally based on adopting *a priori* analytical expression for describing the interface bond-slip law, assuming a fracture process in pure Mode II, disregarding the effect of the interface normal tractions (peeling) and occurrence of out-of-plane displacement (uplift). The interface peeling stress and uplift, experimentally observed through advanced optical systems [34], are developed by eccentricity between applied force and interface. Although, these components affect the ultimate bearing capacity of the adhesive joint, in [35] a negligible influence on the distribution of interface slips throughout the contact has been demonstrated

In the proposed model, incremental analysis with displacements control has been used assuming a bilinear bond-slip law, comparing results with experimental tests and analytical formulations found in the literature.

2 VARIATIONAL FORMULATION

An elastic bar with length L and cross section A attached to an elastic half-plane is considered, as shown in Fig. 1. Reference is made to a Cartesian coordinate system (O, x, z) centred at the middle of the bar, with the vertical axis z directed toward the half-plane and the x-axis placed along the interface. Both the bar and the semi-infinite substrate are made of homogeneous and isotropic solids. Elastic constants E_b and ν_b denote the Young's modulus and Poisson's coefficient of the bar, whereas E_s and ν_s characterise the substrate. Generalised plane stress or plane strain regimes are considered. For plane strain, the width b of the half-plane will be assumed unitary. The thickness of the coating is assumed thin, so making possible to neglect its bending stiffness. Being ignored the peeling stress, only shear tractions $r_x(x)$ occurs along the contact region. The system is subjected to a generically distributed horizontal load $p_x(x)$ or thermal variation $\Delta T(x)$.

Unlike the perfect adhesion case proposed in [23], the relaxed adhesion is representative of the mechanical characteristics of the adhesive connecting the bar with the substrate. This assumption involves different values for the bar displacement $u_{x,b}$ and the half-plane displacement $u_{x,s}$.

2.1 Total potential energy for the bar

The strain energy of a bar can be written as follows:

$$U_{\text{bar}} = \frac{1}{2}\int_L E_0 A(x)\,[u'_{x,b}(x) - \alpha_0 \Delta T]^2 \,\mathrm{d}x, \tag{1}$$

where prime denotes differentiation with respect to x, Young modulus and the coefficient of thermal expansion of the bar are correspondently $E_0 = E_b$, $\alpha_0 = \alpha_b$ for a generalized plane stress or $E_0 =$

$E_b/(1-\nu_b^2)$, $\alpha_0 = (1+\nu_b)\alpha_b$ for a plane strain state. It is worth noting that axial force in the bar is $N(x)$ $= E_0 A(x)[u'_{x,b}(x) - \alpha_0 \Delta T]$. The potential energy Π_{bar} can be written as the strain energy U_{bar} minus the work related to the external loads:

$$\Pi_{\text{bar}} = U_{\text{bar}} - b\int_L [p_x(x) - r_x(x)]\, u_{x,b}(x)\, \mathrm{d}x. \tag{2}$$

2.2 Total potential energy for the substrate

The solution of the elastic problem for a homogeneous isotropic half-plane loaded by a point force tangential to its boundary is referred to as Cerruti solution [36]. In particular, the horizontal displacement $u_{x,s}(x)$ due to the interfacial tractions $r_x(x)$ acting along the boundary between the half-plane and the bar can be found as follows

$$u_{x,s}(x) = \int_L g(x,\hat{x})\, r_x(\hat{x}) d\hat{x}, \tag{3}$$

where the Green function $g(x,\hat{x})$ can be expressed as

$$g(x,\hat{x}) = -\frac{2}{\pi E} \ln \frac{|x-\hat{x}|}{d}. \tag{4}$$

In Eq. (4), $E = E_s$ or $E = E_s/(1-\nu_s^2)$ in the plane stress or plane strain, respectively, and d is an arbitrary length associated with a rigid displacement.

Making use of the theorem of work and energy for exterior domains [37], it can be shown that the total potential energy Π_{soil} for the half-plane equals one half of the work of external loads [23, 24]:

$$\Pi_{\text{soil}} = -\frac{b}{2}\int_L r_x(x)\, u_{x,s}(x)\, \mathrm{d}x \tag{5}$$

By introducing Eq. (3) into Eq. (5) one obtains

$$\Pi_{\text{soil}} = -\frac{b}{2}\int_L r_x(x)\, \mathrm{d}x \int_L g(x,\hat{x})\, r_x(\hat{x})\, \mathrm{d}\hat{x}. \tag{6}$$

2.3 Total potential energy for the adhesive

A jump of displacement occurs when a stiffener is glued to a support by means of an adhesive. In the following, the transmission traction r_x is assumed proportional to the slip $\Delta u_x = u_{x,b} - u_{x,s}$ between the bar and the half-plane displacements

$$r_x = k_x \, \Delta u_x \,, \tag{7}$$

where parameter k_x summarizes the mechanical characteristics of the interface [8]. Making use of Eq. (7), the total potential energy for the adhesive can be written as

$$\Pi_{\text{spring}} = \frac{b}{2} \int_L r_x(x) \, \Delta u_x(x) \, \mathrm{d}\, x - b \int_L r_x(x) \, \Delta u_x(x) \, \mathrm{d}\, x = -\frac{b}{2} \int_L \frac{r_x^2(x)}{k_x} \, \mathrm{d}\, x \tag{8}$$

2.4 Total potential energy for the bar-adhesive-substrate system

Maxing use of Eqs. (2), (6) and (8), the total potential energy of the whole system turns out to be

$$\Pi(u_{x,b}, r_x) = \Pi_{\text{bar}} + \Pi_{\text{soil}} + \Pi_{\text{spring}} \,, \tag{9}$$

which is a mixed variational formulation represented by bar displacement $u_{x,b}$ and interfacial tangential tractions r_x along the contact region. Consequently, making use of Eq. (7), half-plane displacements $u_{x,s} = u_{x,b} - r_x/k_x$.

For a bar attached to an orthotropic substrate having a plane of elastic symmetry coincident with the vertical plane *xz*, in [27] was shown that the orthotropic substrate behaves like an isotropic half-plane assuming an equivalent Young modulus $E = 2 \, c_1/(c_2 \, R_{11})$, where parameters c_1, c_2, R_{11} are reported in Appendix. Obviously, the stress field within the orthotropic substrate differs from that of the isotropic case.

3 FINITE ELEMENT MODEL

Both the bar and the substrate boundary are subdivided into FEs sharing the same mesh. The generic ith FE has a length $l_i = |x_{i+1} - x_{i,}|$ where x_i and x_{i+1} are the initial and end coordinates. Assuming a dimensionless local coordinate $\xi = x/l_i$, nodal displacements $\mathbf{u}_{xi}$ of the bar characterizes completely the axial displacement field in the generic ith FE by means of the vector $\mathbf{N}(\xi)$ containing the shape functions:

$$u_{x,b}(\xi) = [\mathbf{N}(\xi)]^{\mathrm{T}}\, \mathbf{u}_{x,i}\,, \tag{10}$$

In the following, either linear Lagrange polynomials ($N_1 = 1-\xi$, $N_2 = \xi$) or quadratic Lagrange polynomials ($N_1 = 1-3\xi+2\xi^2$, $N_2 = 4\xi(1-\xi)$, $N_3 = \xi(2\xi-1)$) are adopted.

Piecewise constant functions are used to interpolate the tangential tractions

$$r_x(\xi) = [\boldsymbol{\rho}(\xi)]^{\mathrm{T}}\, \mathbf{r}_{x,i}\,, \tag{11}$$

where $\mathbf{r}_{\mathrm{x},i}$ represents the vector of nodal interfacial tangential traction and $\boldsymbol{\rho}(\xi)$ is assumed to be unitary along the generic FE.

Substituting Eqs. (10) and (11) in the variational principle (9) and assembling over all the elements, the potential energy takes the expression

$$\Pi\left(\mathbf{u}_x, \mathbf{r}_x\right) = \frac{1}{2}\mathbf{u}_x^{\mathrm{T}}\mathbf{K}_a\,\mathbf{u}_x - \mathbf{u}_x^{\mathrm{T}}\mathbf{f}_x + \mathbf{u}_x^{\mathrm{T}}\mathbf{H}_{xx}\,\mathbf{r}_x - \frac{1}{2}\mathbf{r}_x^{\mathrm{T}}\mathbf{G}_{xx}\,\mathbf{r}_x - \frac{1}{2}\mathbf{r}_x^{\mathrm{T}}\mathbf{G}_{kx}\,\mathbf{r}_x\ , \tag{12}$$

where $\mathbf{K}_a$ is the bar stiffness matrix and $\mathbf{f}_x$ the external load vector, whose elements take the usual form

$$k_{a,ij} = \frac{1}{l_i}\int_0^1 E_0 A_b(\xi) N_i'(\xi)\, N_j'(\xi)\,\mathrm{d}\,\xi \tag{13}$$

$$f_{x,i} = \int_0^1 \left(N_i(\xi)\, p_x(\xi) b l_i + N_i'(\xi)\, E_0 A(\xi)\,\alpha_0 \Delta T\right)\mathrm{d}\,\xi \tag{14}$$

The components of matrices $\mathbf{H}_{xx}$, $\mathbf{G}_{xx}$ and $\mathbf{G}_{kx}$ are given by the following expressions

$$h_{xx,ij} = b l_i \int_0^1 N_i(\xi)\,\rho_j(\xi)\,\mathrm{d}\xi\,, \tag{15}$$

$$g_{xx,ij} = b \int_{x_i}^{x_{i+1}} \rho_i(x)\,\mathrm{d}x \int_{x_j}^{x_{j+1}} g(x,\hat{x})\,\rho_j(\hat{x})\,\mathrm{d}\hat{x}\,, \tag{16}$$

$$g_{kx,ii} = b \int_{x_i}^{x_{i+1}} \rho_i^2(x) \big/ k_x\,\mathrm{d}x\ . \tag{17}$$

Imposing the potential energy (12) to be stationary, the solution of the problem can be written in the following matrix form

$$\begin{bmatrix} \mathbf{K}_a & \mathbf{H}_{xx} \\ \mathbf{H}_{xx}^{\mathrm{T}} & -(\mathbf{G}_{xx}+\mathbf{G}_{kx}) \end{bmatrix} \begin{Bmatrix} \mathbf{u}_x \\ \mathbf{r}_x \end{Bmatrix} = \begin{Bmatrix} \mathbf{f}_x \\ \mathbf{0} \end{Bmatrix}. \tag{18}$$

The formal solution of the system of equations (18) provides the nodal displacements and tangential tractions

$$\mathbf{r}_x = (\mathbf{G}_{xx}+\mathbf{G}_{kx})^{-1}\,\mathbf{H}_{xx}^{\mathrm{T}}\,\mathbf{u}_x\,, \tag{19}$$

$$(\mathbf{K}_a + \mathbf{K}_{\mathrm{soil}})\,\mathbf{u}_x = \mathbf{f}_x\,, \tag{20}$$

where $\mathbf{K}_{\mathrm{soil}}$ is the stiffness matrix for the substrate with weak interface, defined as:

$$\mathbf{K}_{\mathrm{soil}} = \mathbf{H}_{xx}\,(\mathbf{G}_{xx}+\mathbf{G}_{kx})^{-1}\,\mathbf{H}_{xx}^{\mathrm{T}}. \tag{21}$$

3.1 Prismatic bar subjected to uniform load and thermal variation

A prismatic bar element subjected to uniform loads p_x and thermal variation ΔT is considered. In the case of Lagrange linear functions, bar stiffness matrix $\mathbf{K}_a$, vector of equivalent external load $\mathbf{f}_x$ and matrix $\mathbf{H}_{xx}$ for the ith FE become

$$\mathbf{K}_{a,i} = \frac{E_0 A}{l_i} \begin{bmatrix} 1 & -1 \\ -1 & 1 \end{bmatrix}, \tag{22a}$$

$$\mathbf{f}_{x,i} = p\,b\,l_i/2\,[1,1]^{\mathrm{T}} + E_0 A\,\alpha_0 \Delta T\,[-1,1]^{\mathrm{T}}\,, \tag{22b}$$

$$\mathbf{H}_{xx,i} = b\,l_i/2\,[1,1]^{\mathrm{T}}\,, \tag{22c}$$

whereas for Lagrange quadratic functions become

$$\mathbf{K}_{ai} = \frac{E_0 A}{3 l_i} \begin{bmatrix} 7 & -8 & 1 \\ -8 & 16 & -8 \\ 1 & -8 & 7 \end{bmatrix}, \tag{23a}$$

$$\mathbf{f}_{x,i} = p\, h\, l_i / 6\, [1, 4, 1]^{\mathrm{T}} + E_0 A \alpha_0 \Delta T\, [-1, 0, 1]^{\mathrm{T}} \ , \tag{23b}$$

$$\mathbf{H}_{xx,i} = h\, l_i / 6\, [1, 4, 1]^{\mathrm{T}} \ . \tag{23c}$$

Piecewise constant functions are used to interpolate r_x and the shape functions for the substrate tractions are assumed to be $\boldsymbol{\rho}(\xi) = 1$. Consequently, the components of matrix $\mathbf{G}_{xx}$ are given by

$$g_{xx,ii} = \frac{2b}{\pi E} l_i^2 \left(\frac{3}{2} - \ln l_i \right), \tag{24a}$$

$$\begin{aligned} g_{xx,ij} = \frac{2b}{\pi E} \Big[& \frac{3}{2} l_i l_j + G(x_{j+1} - x_{i+1}) - \\ & G(x_{j+1} - x_i) - G(x_j - x_{i+1}) + G(x_j - x_i) \Big] \quad \text{for } i \neq j, \end{aligned} \tag{24b}$$

where $G(x) = x^2/2\ \ln|x|$ and the contribution due to the arbitrary length d has been omitted since rigid-body displacements can be imposed in post-processing analysis. For instance, the horizontal displacement at one bar end or at the bar midspan can be set to zero.

Finally, the interface adhesive represented by the independent springs is described by a diagonal matrix $\mathbf{G}_{kx}$ having the following components:

$$g_{kx,ii} = \frac{b l_i}{k_{x,i}}, \qquad g_{kx,ij} = 0 \quad \text{for } i \neq j \ , \tag{25a, b}$$

where $k_{x,i}$ is stiffness value of the generic ith FE.

3.2 Solution and post-processing

The solution of the FE-BIE analysis, i.e., the system of equations (18), gives nodal displacement of the bar $\mathbf{u}_x$ and substrate traction $\mathbf{r}_x$. Once the nodal values of the primary variables are known, the axial force $N = E_0 A\,(u'_{x,b} - \alpha_0 \Delta T)$ and the displacement of the substrate $u_{x,s} = u_{x,b} - r_x/k_x$.

In summary, the general flow of the analysis of a reinforcement bar resting on an elastic substrate requires that the following steps be taken:

- discretize the bar element and the underlying substrate into FEs;
- calculate element matrices $\mathbf{K}_{ai}$, $\mathbf{H}_{xx,i}$ and vectors $\mathbf{f}_{x,i}$ for every element;
- assemble element matrices $\mathbf{K}_{ai}$ and vectors $\mathbf{f}_{x,i}$ into the global matrix $\mathbf{K}_a$ and vector $\mathbf{f}_x$;
- assemble element matrices $\mathbf{H}_{xx,i}$ into the global matrix $\mathbf{H}_{xx}$;
- calculate global matrix $\mathbf{G}_{xx}$ and $\mathbf{G}_{kx}$;
- solve the system of equation (18) for the primary variables $\mathbf{u}_x$ and $\mathbf{r}_x$;
- compute secondary variables $u_{x,s}$ and N.

4 NUMERICAL EXAMPLES

Similarly to [4, 23], the elastic response of the bar-substrate system is characterised by the parameter

$$\beta L = \frac{E\,b\,L}{E_0 A}. \tag{26}$$

Low values of βL characterise short bars stiffer than the substrate. In this case, the bar performs like an almost inextensible stiffener. Higher values of βL describe long bars bonded to stiff substrate. With regards to the weak interface, the following parameter is introduced:

$$\gamma L = \sqrt{\frac{k_x\,b\,L^2}{E_0 A}}\,. \tag{27}$$

Low values of γL characterise practically detached bars, whereas high values of γL correspond to almost perfectly attached bars.

In the present section, several loading cases of a bar weakly attached to the underlying half-plane are considered and discussed. In the first part, some common problems are studied assuming a linear elastic behaviour of the bond-slip law and comparisons with the perfect bonded case are made. In the second part, debonding of a FRP glued on a concrete substrate is analysed. Numerical results are compared with solutions and experimental tests found in the literature.

4.1 Linear analysis

In the following, a number of 512 equal FEs having quadratic Langrange polynomials are used to model the elastic bar. A bar subjected to a horizontal concentrated force P_x, or a uniform thermal variation is analysed.

4.1.1 Bar loaded by a horizontal point force P_x at one end

A flexible bar loaded by a horizontal point force P_x at one end is investigated for the case $\beta L = 10$, $\gamma L = 5$ and $\gamma L = \infty$ (perfect adhesion). Dimensionless values of displacements, axial forces and tangential tractions along the bar are reported in Fig. 2. With reference to the weak interface case, bar displacements $u_{x,b}$ increase and substrate displacements $u_{x,s}$ decrease along the whole contact region with respect to the perfect adhesion case (Fig. 2a). Axial force tends to become higher along the bar (Fig. 2b) and the tangential tractions are not singular at the bar ends as occurs with regard to those ones in the perfect adhesion case (Fig. 2c). Fig. 3 shows maximum tangential reaction $r_x(L/2)$ versus parameter γL. It is worth noting that the value of the maximum traction depends on γL almost linearly irrespective of the parameter βL. In particular, $r_x(L/2) = C\,\gamma\,P_x$, where $C = 1$ for $\beta L \geq 10$ and $\gamma L \geq 3$ and $C = 1.19$ for $\beta L = 1$ and $\gamma L \geq 4$.

4.1.2 Bar subjected to an uniform thermal variation

In this section, an elastic bar subjected to a uniform thermal variation is investigated. This case is similar to that of a bar symmetrically loaded by two equal opposite force applied at the ends [5]. In particular, the axial displacement and the interfacial tangential traction of a bar subject to a uniform thermal load ΔT coincide with those induced in the bar by two opposite axial forces of magnitude $P_x = E_0 A \alpha_0 \Delta T$ applied at the ends [5]. As for the discrete problem and assuming consecutive bar FEs, the vector of equivalent external loads, where the components of the generic ith FE is reported in Eq. (23b), reduces to $\mathbf{f}_x = P_x [-1, 0, ..., 0, 1]^T$. The axial force of a bar which is subjected to two opposite forces P_x is equal that of the same bar subjected to a thermal load ΔT increased by the quantity $E_0 A \alpha_0 \Delta T$.

Nondimensional value of u_x, N and r_x versus x/L are reported in Fig. 4 for the case $\beta L = 10$, $\gamma L = 5$ and $\gamma L = \infty$ (perfect adhesion). For the weak interface case, the bar displacements u_{xb} increase while substrate displacements u_{xs} decrease with respect to the perfect adhesion case (Fig. 4a). The magnitude of the axial force N diminishes (Fig. 4b) and tangential tractions r_x result more distributed along the bar annihilating the tractions singularity close to the bar ends (Fig. 4c).

4.2 Incremental nonlinear analysis of a shear-out test

In the scientific literature, several shear-out tests are available, especially for FRP strengthened RC structures [32, 38]. The shear-out tests could be used to determine not only the ultimate bearing capacity but even the local bond-slip behaviour of the interface [39, 40]. The bilinear elastic-softening bond-slip relationship is the most commonly function adopted [41].

In this section, the debonding process in shear-out test due to an horizontal force P_x applied at the right bar end is evaluated using an incremental analysis with displacement control. The debonding phenomenon occurs when the slip between the strip and substrate attains a critical value that causes separation. Fracture behaviour in pure Mode II is assumed throughout the interface that is characterised by a bilinear elastic-softening bond-slip relationship (Fig. 5). A linear ascending

branch, which is described by the stiffness parameter $k_{x,E,}$ reaches the elastic limit $r_{x,0}$ at the elastic slip limit $\Delta u_{x,e} = r_{x,0}/k_{x,E}$. Afterwards a linear softening branch with descending slope $k_{x,S}$ is activated. At the end, beyond the ultimate slip $\Delta u_{x,u} = r_{x,0}/k_{x,E} + r_{x,0}/k_{x,S}$, no bond tractions can be transferred trough the interface.

The mechanical and geometrical proprieties proposed in [10, 41] are introduced basing on experimental results reported in [42]. In particular, the elastic modulus of the Carbon FRP (CFRP) plate is E_0 = 100 GPa, while b = 25.4 mm and A = 25 mm^2. For the concrete substrate E = 30 GPa. Two specimens in plane stress state characterised by bond lengths 50 and 200 mm are analysed, having parameter βL equal to 15 and 61, respectively. A number of 64 equal FEs having linear Langrange polynomials are used to model the shorter bar (50 mm), while 128 equal FEs are used for the second one (200 mm), which can describe the behaviour of a long bar.

Because of the randomness of the mechanical properties of the concrete substrate, the calibration procedure outlined in [40] assumes that each specimen has different interface properties. For the short anchorage, traction limit $r_{x,0}$ = 6.9 MPa with stiffness $k_{x,E}$ = 135 N/mm^3 (γL = 1.9), $k_{x,S}$ = 25 N/mm^3 and ultimate slip $\Delta u_{x,u}$ = 0.33 mm are assumed, whereas for the long anchorage, $r_{x,0}$ = 5.0 MPa with $k_{x,E}$ = 5000 N/mm^3 (γL = 38), $k_{x,S}$ = 100 N/mm^3 and $\Delta u_{x,u}$ = 0.05 mm.

Fig. 6 shows the applied force P_x versus the maximum slip Δu_x, FRP axial strain $\varepsilon_{x,\mathrm{FRP}}$ and interface tangential traction r_x throughout the bonding length for the short and long anchorages. Cartesian coordinate system (O, x, z) is centred at the left bar end. The force-slip response of the short anchorage is shown in Fig. 6a, where dashed line with symbol × refers to the closed-form analysis proposed in [10], assuming a rigid substrate. As a result, the substrate elasticity taken into account by the proposed FE-BIE model reduces the maximum slip from those calculated through a model with rigid support. The corresponding values of the FRP axial strains $\varepsilon_{x,\mathrm{FRP}}$ throughout the bond length are shown in Fig. 6b, for the elastic state (solid line) and the softening state (dashed line). An exponential shape of the axial strain $\varepsilon_{x,\mathrm{FRP}}$ can be observed until the maximum load $P_{x,\mathrm{D}}$ (i.e. point D in Fig. 6a) is attained. Subsequently, the trend of $\varepsilon_{x,\mathrm{FRP}}$ becomes linear and decreases

until a complete detachment is achieved. Poor agreement between numerical predictions and experimental $\varepsilon_{x,FRP}$ has been found. Indeed, the assumed bond law parameters work well with a rigid substrate [10], where the elastic concrete deformation close to the interface has been taken into account implicitly. Numerical models adopting two-dimensional substrate require adjustment of the interface laws calibrated by using one-dimensional model [22]. The main aim of the present example is to show how the proposed FE-BIE method is simple and effective. Nonetheless, a subsequent research may be devoted to find the interface law suitable for the proposed FE-BIE method. The evolution of the interface shear tractions r_x is clearly reported in Fig. 6c. In early stages, an exponential shape of traction is shown along the contact region. A transition stage starts when traction $r_x(L) = r_{x,0}$, i.e., line B in Fig. 6c, and it continues until every reactions overtake the traction limit $r_{x,0}$, i.e., line D in Fig. 6c. Finally, a progressive decrease in reactions occurs up to an achievemnet of the complete debonding.

The force-slip response of long anchorage is shown in Fig. 6d, where a constant plateau has been emerged. Results similar to those reported in [10] have been obtained, with the exception of largest plateau displacements. This aspect may depend on different choices of stiffness parameters of the interface law, which are not clearly stated in [10]. The FRP axial strains $\varepsilon_{x,FRP}$ and the substrate reaction are reported in Figs. 6e and 6f, respectively, for the elastic state (solid line) and the softening state (dashed line). Points A in Fig. 6d characterise the end of the elastic states, whereas points B, C, D symbolise the elastic-softening behaviours. Subsequently, the debonding states begin at points E and continue until points G. In the detachment zone, the FRP axial strains $\varepsilon_{x,FRP}$ remains constant and does not increase. The tangential tractions r_x are reported in Fig. 6f, where a progressive decrease in tractions occurs up to attainment of the complete debonding.

5 CONCLUSIONS

A simple and effective FE-BIE method has been proposed to investigate problems of axially loaded bar weakly attached to a homogeneous elastic substrate. Bar FEs has been used to simulate thin

structures, whereas the behaviour of the semi-infinite substrate has been represented using a BIE. Making use of a mixed variational formulation including the Green function of the half-plane, the axial displacement of the bar is interpolated using first or second order Lagrange polynomials, whereas the interfacial shear traction is approximated by piecewise constant functions. A slip between the flexible bar and the elastic substrate is introduced using a set of independent springs.

Several examples have been presented to show the effectiveness of the proposed formulation. Firstly, linear elastic analyses has been performed. In particular, tangential traction and axial force of a bar subjected to horizontal point force or uniform thermal variation has been investigated. Secondly, incremental nonlinear analysis with displacement control has been used to study the delamination of a reinforcement bar glued to a substrate. The mechanical behaviour of the adhesive is described through a bond-slip law which is assumed *a priori*. Both short and long anchorages has been investigated showing the difference in terms of tangential tractions and axial strains throughout the bonded length or in term of the global response outlined by the plot of the applied force versus the maximum slip. The influence of the substrate elasticity is made by means of comparison with model adopting a rigid substrate. Poor agreement with experimental FRP axial strains has been found due to the use of parameters calibrated for one-dimensional model. Indeed, two-dimensional substrate requires adjustment of the elastic stiffness to be used in the bond-slip law. This aspect is well known as the bond-slip law is particularly sensitive to the adopted numerical model. A subsequent research may be devoted to find the bond-slip model to be adopted in the proposed FE-BIE method.

ACKNOWLEDGMENTS

The present investigation was developed in the framework of the Italian PRIN Fund No. 2015LYYXA8 and of the Research Program FAR 2017 of the University of Ferrara. Moreover, the analyses were developed within the activities of the (Italian) University Network of Seismic

Engineering Laboratories–ReLUIS in the research program funded by the (Italian) National Civil Protection – Progetto Esecutivo 2014-2018 – Research Line “Reinforced Concrete Structures”.

APPENDIX

In plane stress state, the substrate coefficients c_1, c_2, R_{11} are given by

$$c_1 = \left(\frac{E_z}{E_x}\right)^{1/4}, \quad c_2 = \left(2 + \frac{\sqrt{E_x E_z}}{G_{xz}} - 2\,\nu_{xz}\left(\frac{E_z}{E_x}\right)^{1/2}\right)^{1/2}, \quad R_{11} = \frac{1}{E_x}, \tag{A.1a,b,c}$$

whereas in plane strain state the constants c_1, c_2, R_{11} become

$$c_1 = \left(\frac{E_z}{E_x}\frac{1-\nu_{xy}\nu_{yx}}{1-\nu_{zy}\nu_{yz}}\right)^{1/4}, \tag{A.2a}$$

$$c_2 = \left(2 + \sqrt{\frac{E_z}{(1-\nu_{xy}\nu_{yx})(1-\nu_{zy}\nu_{yz})}}\left(\frac{\sqrt{E_x}}{G_{xz}} - \frac{2(\nu_{xz}+\nu_{xy}\nu_{yz})}{\sqrt{E_x}}\right)\right)^{1/2}, \tag{A.2b}$$

$$R_{11} = \frac{1-\nu_{xy}\nu_{yx}}{E_x}. \tag{A.2c}$$

where E_i denotes the Young's modulus along the directions $i = x, z$, G_{ij} and ν_{ij} are the shear modulus and Poisson's coefficient, respectively, associated with the pair directions $i, j = x, y, z$. In particular, due to this special kind of material symmetry, $\nu_{ij}/E_i = \nu_{ji}/E_j$. For an isotropic substrate, the coefficients reduce to $c_1 = 1$, $c_2 = 2$.

REFERENCES

[1] Bakis C, Bank L, Brown V, Cosenza E, Davalos J, Lesko J, Machida A, Rizkalla S, Triantafillou T. Fiber-reinforced polymer composites for construction - State of the art review. J Compos Constr 2002;6(2):73–87.

[2] Zhao X L, Zhang L. State of the art review on FRP strengthened steel structures. Eng Struct 2007;29(8):1808–23.

[3] Teng JG, Chen JF, Smith ST, Lam L. FRP strengthened RC structures. Chichester: John Wiley & Sons; 2001.

[4] Grigolyuk EI, Tolkachev VM. Contact problems in the theory of plates and shells, Mir Publishers, Moscow 1987.

[5] Lanzoni L. Analysis of stress singularities in thin coatings bonded to a semi-infinite elastic substrate. Int J Solids Struct 2011;48(13):1915–1926.

[6] Lenci S. Melan's problems with weak interface, J Appl Mech - Trans ASME 2000;67(1):22–28.

[7] Goland M, Reissner E. The stresses in cemented joints. J Appl Mech - Trans ASME 1944;11:A17–A27.

[8] Geymonat G, Krasucki F, Lenci S. Mathematical analysis of a bonded joint with soft thin adhesive, Math Mech Solids 1999;4(2):201–225.

[9] Rizzoni R, Dumont S, Lebon F, Sacco E. Higher order model for soft and hard elastic interfaces. Int J Solids Struct 2014;51(1):4137-4148.

[10] Caggiano A, Martinelli E, Faella C. A fully-analytical approach for modelling the response of FRP plates bonded to a brittle substrate. Int J Solids Struct 2012;49(17):2291–2300.

[11] Franco A, Royer-Carfagni G. Cohesive debonding of a stiffener from an elastic substrate. Compos Struct 2014; 111:401–414.

[12] Franco A, Royer-Carfagni G. Effective bond length of FRP stiffeners. Int J Non-Linear Mech 2014;60:46–57.

[13] Rabinovitch O. Fracture-mechanics failure criteria for RC beams strengthened with FRP strips – a simplified approach. Compos Struct 2004;64(3–4):479–492.

[14] Wu Z, Yin J. Fracturing behaviors of FRP-strengthened concrete structures. Eng Fract Mech 2003;70(10):1339–1355.

[15] Lu XZ, Ye LP, Teng JG, Jiang JJ. Meso-scale finite element model for FRP sheets/plates bonded to concrete. Eng Struct 2005;27(4):564–575.

[16] Benzarti K, Freddi F, Frémond F. A damage model to predict the durability of bonded assemblies. Part I: Debonding behaviour of FRP strengthened concrete structures. Constr Build Mater 2011;25(2):547–555.

[17] Benvenuti E, Vitarelli O, Tralli A. Delamination of FRP-reinforced concrete by means of an extended finite element formulation. Compos Part B Eng 2012;43(8):3258–3269.

[18] Benvenuti E, Orlando N, Ferretti D, Tralli A. A new 3D experimentally consistent XFEM to simulate delamination in FRP-reinforced concrete. Compos Part B Eng 2016;91:346–360.

[19] Zhang Y-M, Gu Y, Chen J-T. Internal stress analysis for single and multilayered coating systems using the boundary element method. Eng Anal Bound Elem 2011; 35(4):708–717.

[20] Gu Y, Chen W, Zhang B. Stress analysis for two-dimensional thin structural problems using the meshless singular boundary method. Eng Anal Bound Elem 2015; 59:1–7.

[21] Salvadori A. A symmetric boundary integral formulation for cohesive interface problems. Comput Mech 2003;32(4–6):381–391.

[22] Freddi F, Savoia M. Analysis of FRP–concrete debonding via boundary integral equations. Eng Fract Mech 2008;75(6):1666–1683.

[23] Tullini N, Tralli A, Lanzoni L. Interfacial shear stress analysis of bar and thin film bonded to 2D elastic substrate using a couple FE-BIE method. Finite Elem Anal Des 2012;55:42–45.

[24] Tullini N, Tralli A. Static analysis of Timoshenko beam resting on elastic half-plane based on the coupling of locking-free finite elements and boundary integral. Comput Mech 2010;45(2–3):211–225.

[25] Baraldi D, Tullini N. Incremental analysis of elasto-plastic beams and frames resting on an elastic half-plane. J Eng Mech 2017; 134(9): Article number 04017101, 1-9.

[26] Tezzon E, Tullini N, Minghini M. Static analysis of shear flexible beams and frames in adhesive contact with an isotropic elastic half-plane using a coupled FE-BIE model. Eng Struct 2015;104:32–50.

[27] Tezzon E, Tullini N, Lanzoni L. A coupled FE-BIE model for the static analysis of Timoshenko beams bonded to an orthotropic elastic half-plane. Eng Anal Bound Elem 2016;71:112–128.

[28] Tullini N, Tralli A, Baraldi D. Stability of slender beams and frames resting on 2D elastic half-space. Arch Appl Mech 2013;83(3):467–482.

[29] Tullini N, Tralli A, Baraldi D. Buckling of Timoshenko beams in frictionless contact with an elastic half-plane. J Eng Mech 2013; 139(7): 824–831.

[30] Kikuchi N, Oden J. Contact problems in elasticity: A study of variational inequalities and finite element methods, SIAM, Philadelphia, 1988.

[31] Bielak J, Stephan E. A modified Galerkin procedure for bending of beams on elastic foundations, SIAM J Sci Stat Comput 1983; 4(2): 340–352.

[32] Ferracuti B, Mazzotti C, Savoia M. A new single-shear set-up for stable debonding of FRP–concrete joints. Constr Buil Mater 2008;23(4):1529–1537.

[33] Panigrahi S, Pradhan B. Onset and growth of adhesion failure and delamination induced damages in double lap joint of laminated FRP composites. Compos Struct 2008;85(4):326–336.

[34] Czaderski C, Soudki K, Motavalli M. Front and side view image correlation measurements on FRP to concrete pull-off bond tests. J Compos Constr 2010;14(4):451–464.

[35] Martinelli E, Czaderski C, Motavalli M. Modeling in-plane and out-of-plane displacement fields in pull-off tests on FRP strips. Eng Struct 2011;33(12):3715–3725.

[36] Johnson K L. Contact Mechanics, University Press, Cambridge, 1985.

[37] Gurtin ME, Sternberg E. Theorems in linear elastostatics for exterior domains, Arch Ration Mech Anal 1961;8(1):99–119.

[38] Yao J, Teng JG, Chen JF. Experimental study on FRP to concrete bonded joints. Compos Part B Eng 2005;36(2):99–113.

[39] Taljsten B. Defining anchor lengths of steel and CFRP plates bonded to concrete. Int J Adhes Adhes 1997;17(4):319–327.

[40] Lu XZ, Teng JG, Ye LP, Jiang JJ. Bond–slip models for FRP sheets/plates bonded to concrete, Eng Struct 2005; 27: 920–937.

[41] Faella C, Martinelli E, Nigro E. Direct versus indirect method for identifying FRP to concrete interface relationships. J Compos Constr 2009;13(3):226–233.

[42] Chajes MJ, Finch WW, Januska TF, Thomson TA. Bond and force transfer of composite material plates bonded to concrete. ACI Struct J 1996;93(2):208–217.

Figure Captions

Fig. 1. Bar weakly attached on semi-infinite substrate (**a**), and free-body diagram (**b**).

Fig. 2. Bar loaded by a point force P_x at one end. Nondimensional values of u_x (**a**), N (**b**) and r_x (**c**) versus x/L for $\beta L = 10$, $\gamma L = 5$ (solid line) and $\gamma L = \infty$ (dashed line - perfect adhesion).

Fig. 3. Bar loaded by a point force P_x at one end. Nondimensional values of r_x at the end ($x/L = 0.5$) versus γL.

Fig. 4. Bar subjected to a uniform thermal variation ΔT. Nondimensional values of u_x (**a**), N (**b**) and r_x (**c**) versus x/L for $\beta L = 10$, $\gamma L = 5$ (solid line) and $\gamma L = \infty$ (dashed line - perfect adhesion).

Fig. 5. Bilinear bond-slip law.

Fig. 6. Incremental nonlinear analysis of a shear-out test of short (**a**, **b**, **c**) (L = 50 mm) and long (**d**, **e**, **f**) anchorage. Applied force P_x vs. the maximum slip Δu_x (**a**, **d**), FRP axial strain $\varepsilon_{x,\mathrm{FRP}}$ (**b**, **e**) and interface shear stress r_x (**c**, **f**) along the bonding length. Results reported by Caggiano et al. (dashed line with symbol (×) in (**a**)) and experiment tests reported by Chajes et al. (dots in (**b**)).

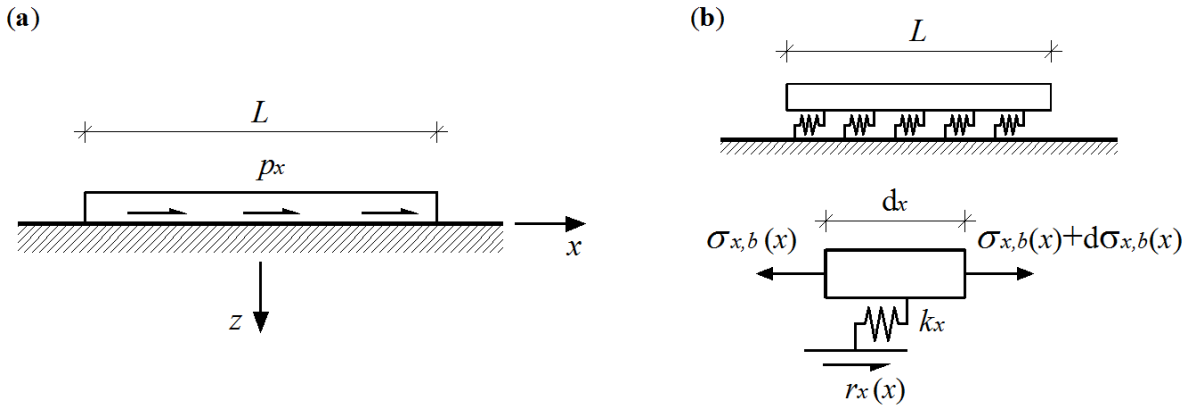

Fig. 1. Bar weakly attached on semi-infinite substrate (**a**), and free-body diagram (**b**).

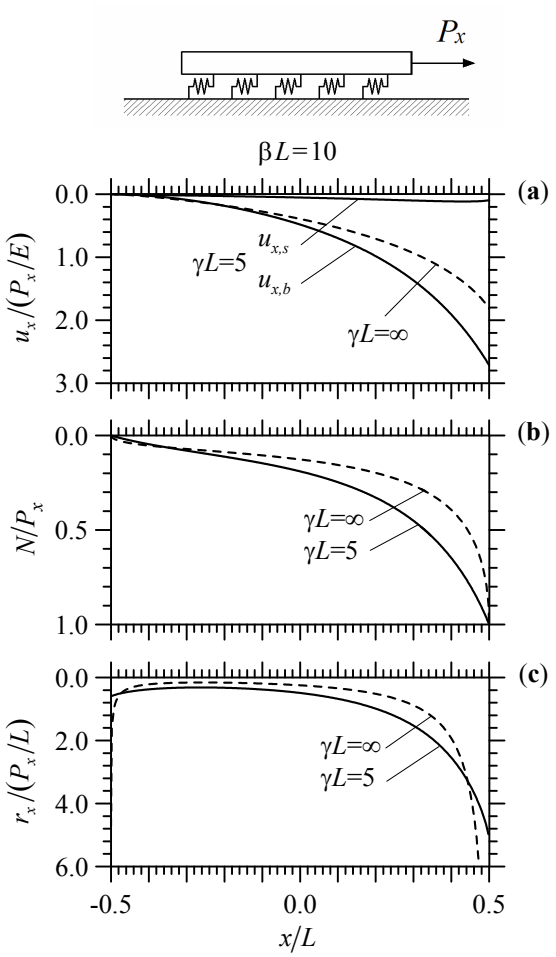

Fig. 2. Bar loaded by a point force P_x at one end. Nondimensional values of u_x (**a**), N (**b**) and r_x (**c**) versus x/L for $\beta L = 10$, $\gamma L = 5$ (solid line) and $\gamma L = \infty$ (dashed line - perfect adhesion).

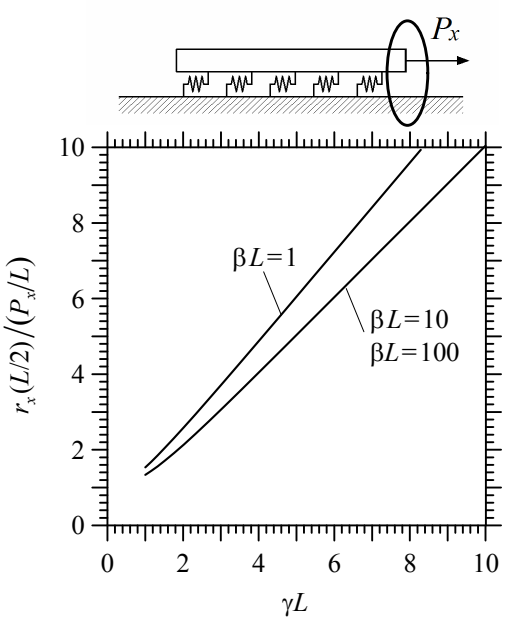

Fig. 3. Bar loaded by a point force P_x at one end. Nondimensional values of r_x at the end ($x/L = 0.5$) versus γL.

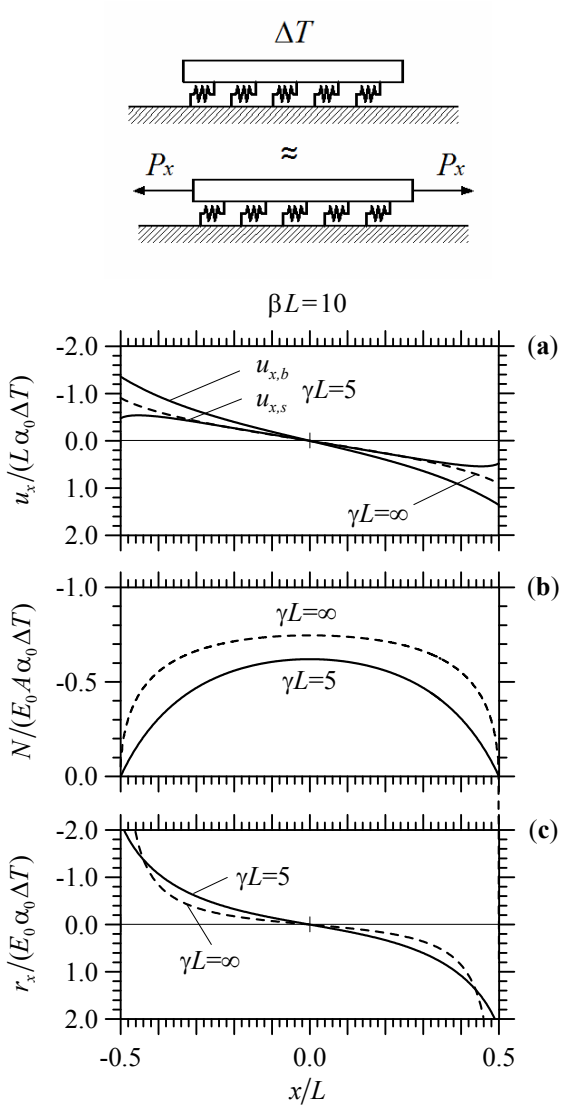

Fig. 4. Bar subjected to a uniform thermal variation ΔT. Nondimensional values of u_x (**a**), N (**b**) and r_x (**c**) versus x/L for $\beta L = 10$, $\gamma L = 5$ (solid line) and $\gamma L = \infty$ (dashed line - perfect adhesion).

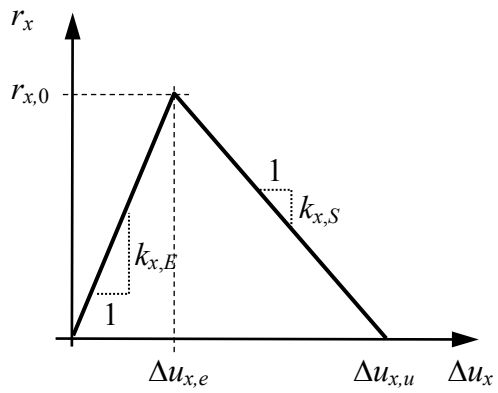

Fig. 5. Bilinear bond-slip law.

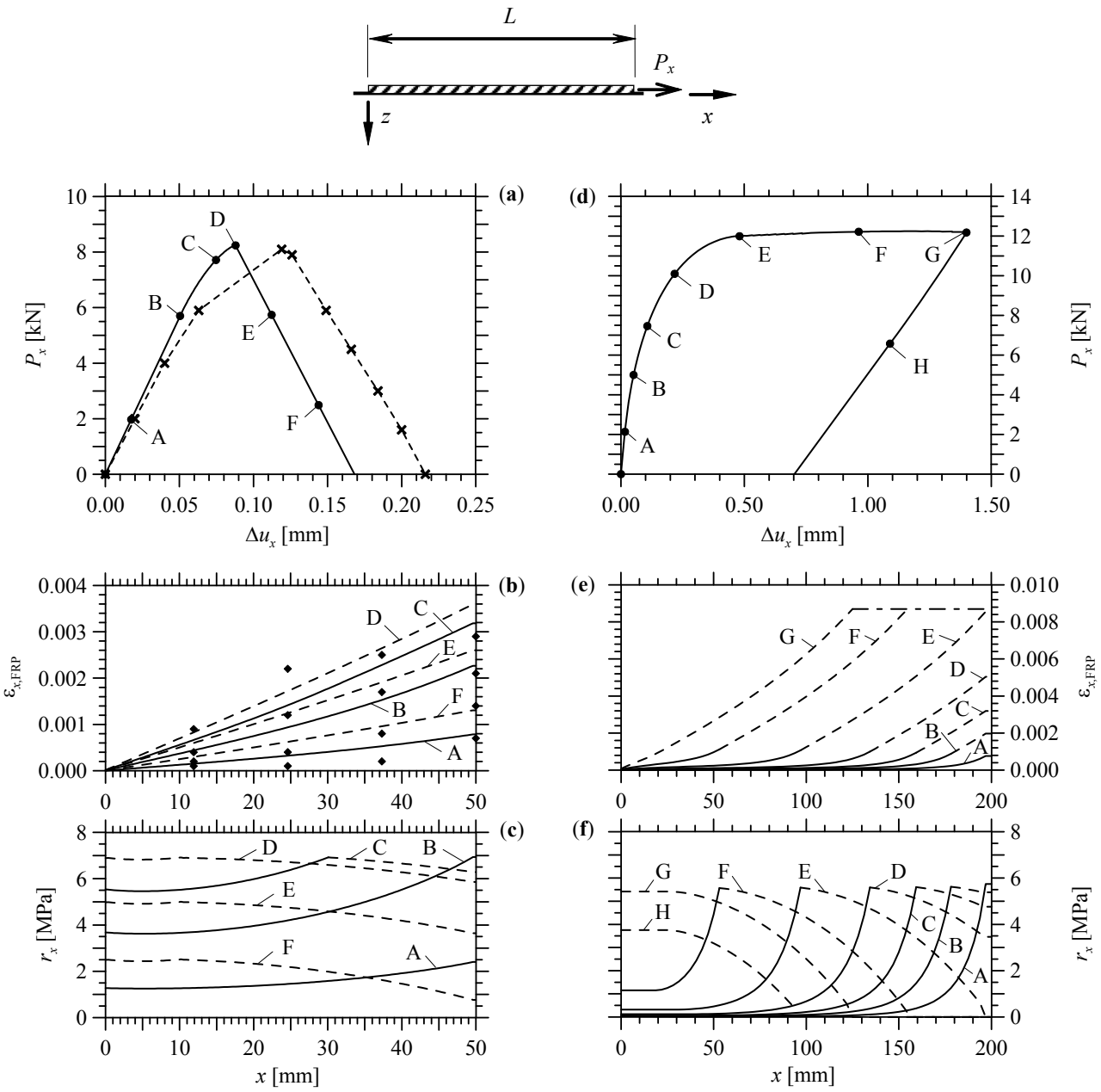

Fig. 6. Incremental nonlinear analysis of a shear-out test of short (**a**, **b**, **c**) (L = 50 mm) and long (**d**, **e**, **f**) anchorage. Applied force P_x vs. the maximum slip Δu_x (**a**, **d**), FRP axial strain $\varepsilon_{x,\mathrm{FRP}}$ (**b**, **e**) and interface shear stress r_x (**c**, **f**) along the bonding length. Results reported by Caggiano et al. (dashed line with symbol (×) in (**a**)) and experiment tests reported by Chajes et al. (dots in (**b**)).